Electronic Supplementary Material (ESI) for CrystEngComm.

Supporting Information

Two new luminescent Cd(II)-based coordination polymers by regulating the asymmetrical tetracarboxylate and auxiliary ligands displaying high sensitivity for Fe^{3+} and CrO_4^{2-}

Materials and Method

All the reagents to perform synthesis were obtained from commercial sources and were used without further purification. Powder X-ray diffraction (PXRD) data were collected using Bruker ADVANCE X-ray diffractometer with Cu-Kα radiation (λ=1.5418 Å) at 50 kV, 20 mA with a scanning rate of 6°/min and a step size of 0.02°. Fourier transform infrared (FT-IR) spectra for both the coordination polymers as KBr discs were recorded on Nicolet Impact 750 FTIR in the range of 400-4000 cm^{-1}. Thermogravimetric analyses (TGA) were performed under nitrogen atmosphere from room temperature to 900 °C at a heating rate of 10 °C min^{-1}. The sensor investigations were carried out on spectrophotometer.

X-ray Crystallography

The single crystal X-ray diffraction data for both coordination polymers were collected on a Bruker SMART APEX diffractometer which was equipped with graphite monochromated MoKα radiation (λ = 0.71073 Å) by using an ω-scan technique. The structures were solved by direct method (SHLEXS-2014) and refined using the full-matrix least-square procedure based on F^2 (Shelxl-2014) [1]. All the hydrogen atoms were generated geometrically and refined isotropically using a riding model. All non-hydrogen atoms were refined with anisotropic displacement parameters. Crystallographic details and selected bond dimensions for **1**-**2** are listed in Tables S1-S3, respectively. CCDC numbers: 2049745-2049746.

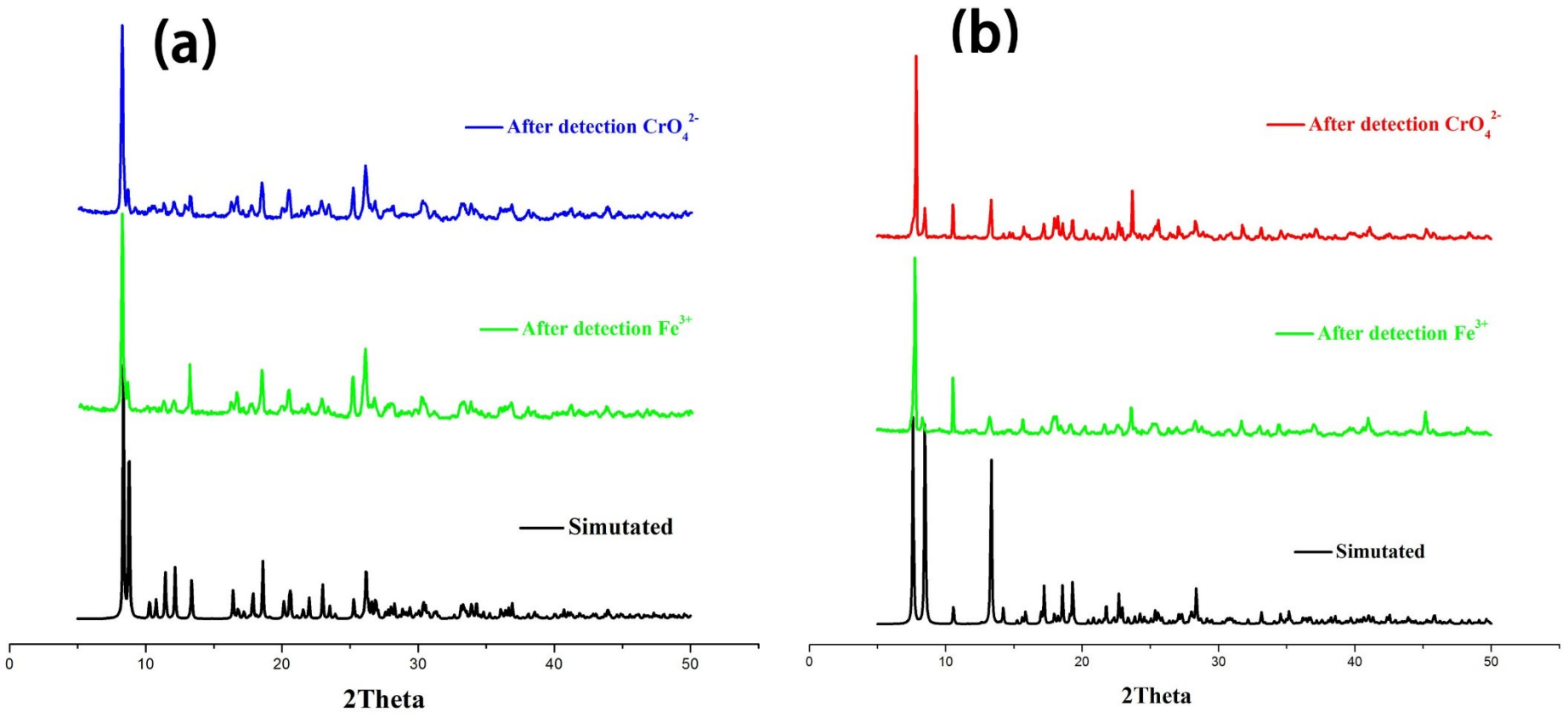

Fig. S1 (a) and (b) Powder XRD patterns of the simulated diagram from single crystal data (black), after detection Fe^{3+} (green) and after detection CrO_4^{2-}(blue and red) for **1**-**2**, respectively.

FTIR spectroscopy

In the FTIR spectra it displayed strong and broad stretching vibrations at ca. 3480 cm^{-1}, which can be assigned to the vibrations arising from the water molecules in **2** (Fig. S2). There is not any band around 1700 cm^{-1} in **1** indicates that the H_4L ligands are completely deprotonated. The intense bands

observed at ca. 1650 and 1420 cm^{-1} arises because of the asymmetric stretching and symmetric vibration of the carboxylate group of H_4L ligands, respectively. The value differences of $\nu_{as(COO)}-\nu s_{(COO)}$ suggest that the H_4L ligands adopts bidentate and monodentate coordination modes, respectively. Additionally, the band observed at ca. 1520 cm^{-1} can be ascribed to the C=N stretching vibrations of N-donor ligand.

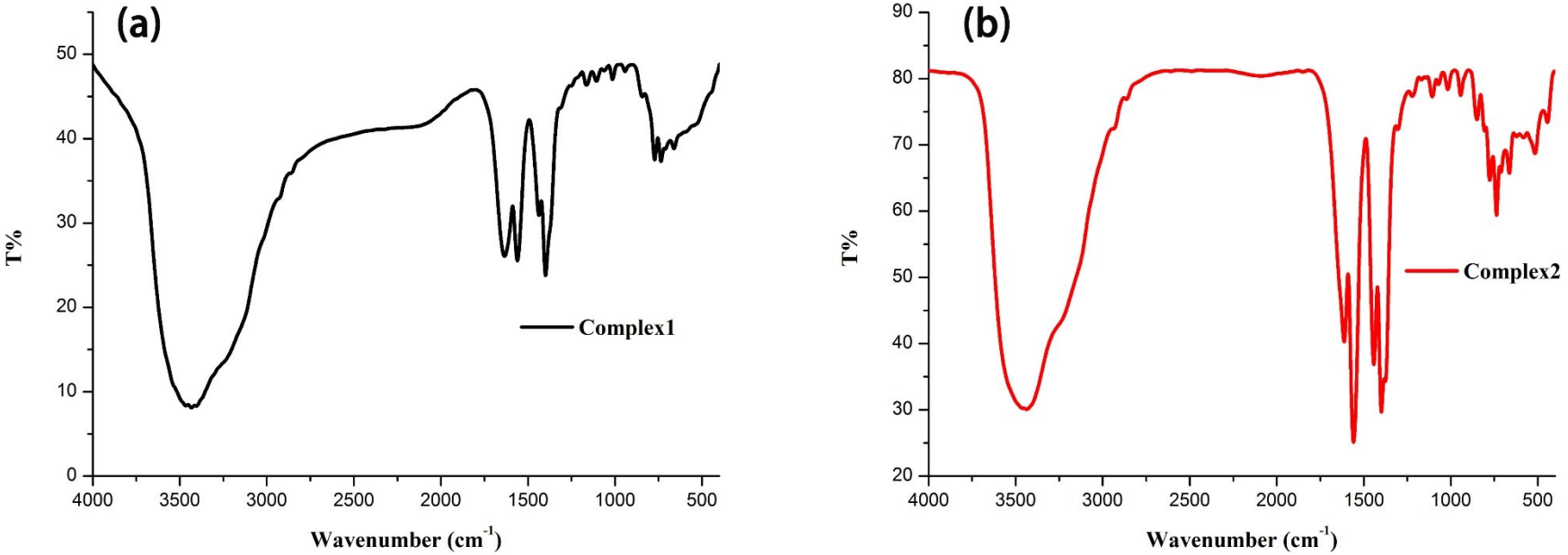

Fig. S2 view of the IR.

Thermal analyses

To evaluate the thermal stability of complexes **1–2**, thermogravimetric (TG) analysis of complexes was performed under N_2 conditions from room temperature to 800 °C with a heating rate of 5 °C min^{-1} (Fig. S3). Complex **2** displayed two weight loss stages. The first weight loss stage from 30 to 256 °C results from the complete decomposition of the coordinated H_2O molecules (obsd: 11.8%, calcd: 11.6%). The second weight loss stage from 406 to 550 °C results from the decomposition of the organic ligands. Complex **1** can be stabilized until 460 °C.

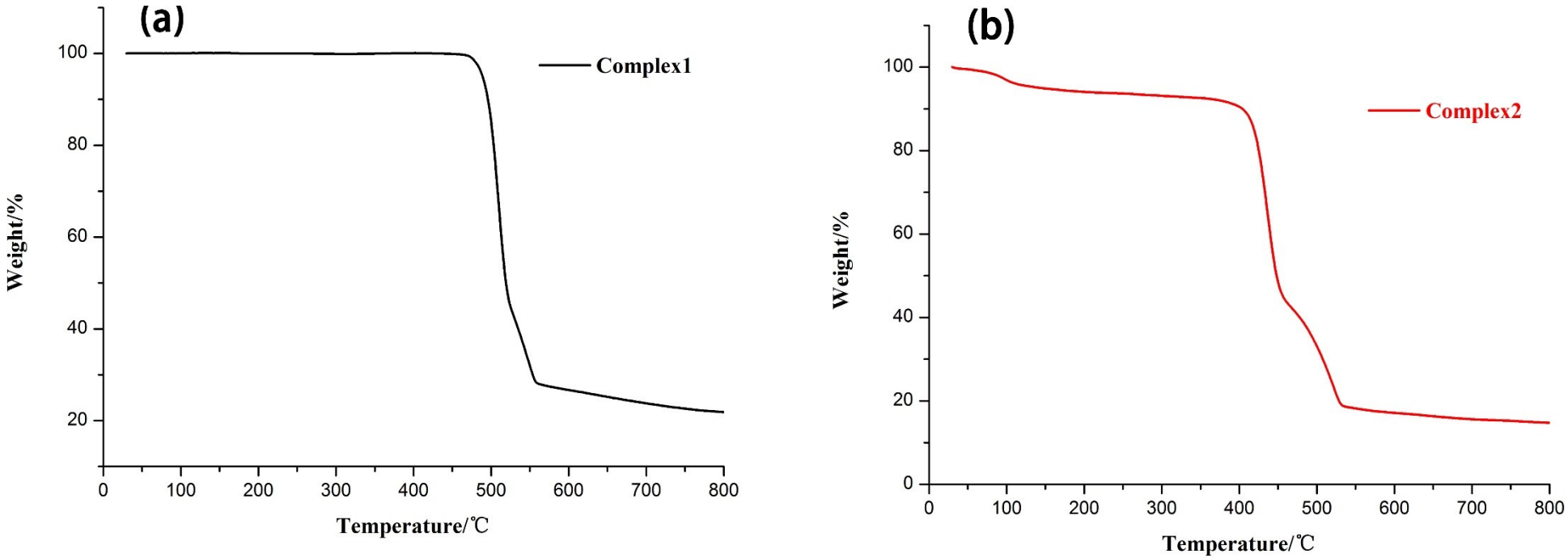

Fig. S3 view of the TGA.

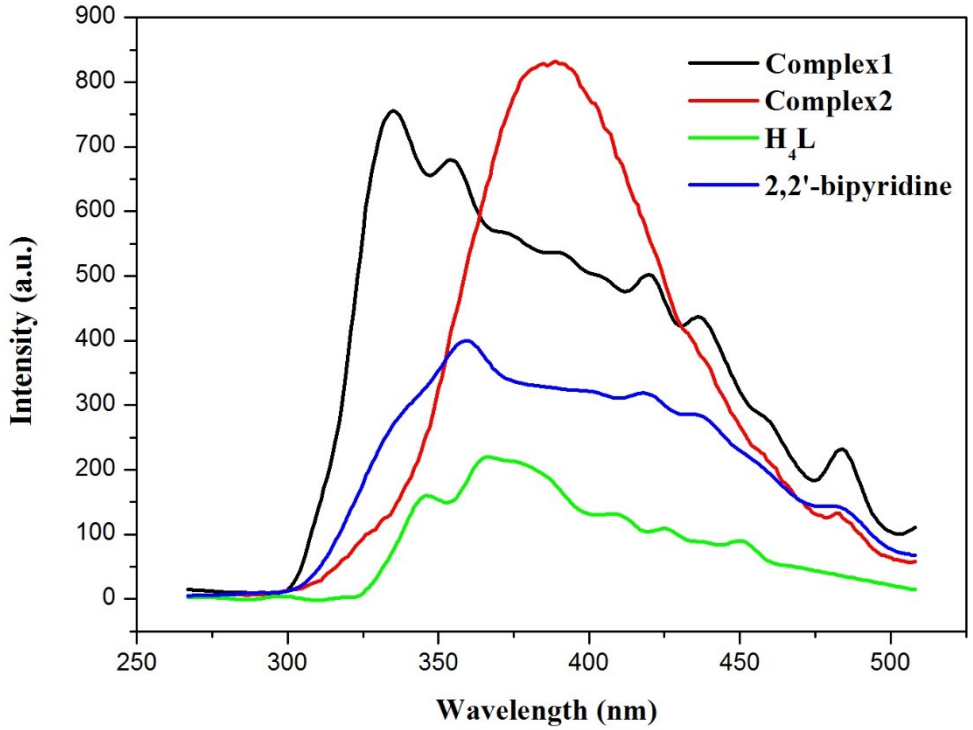

Fig. S4 Luminescence emission spectra of the CPs and the ligands (λex = 260 nm for **1**, 265 nm for **2**).

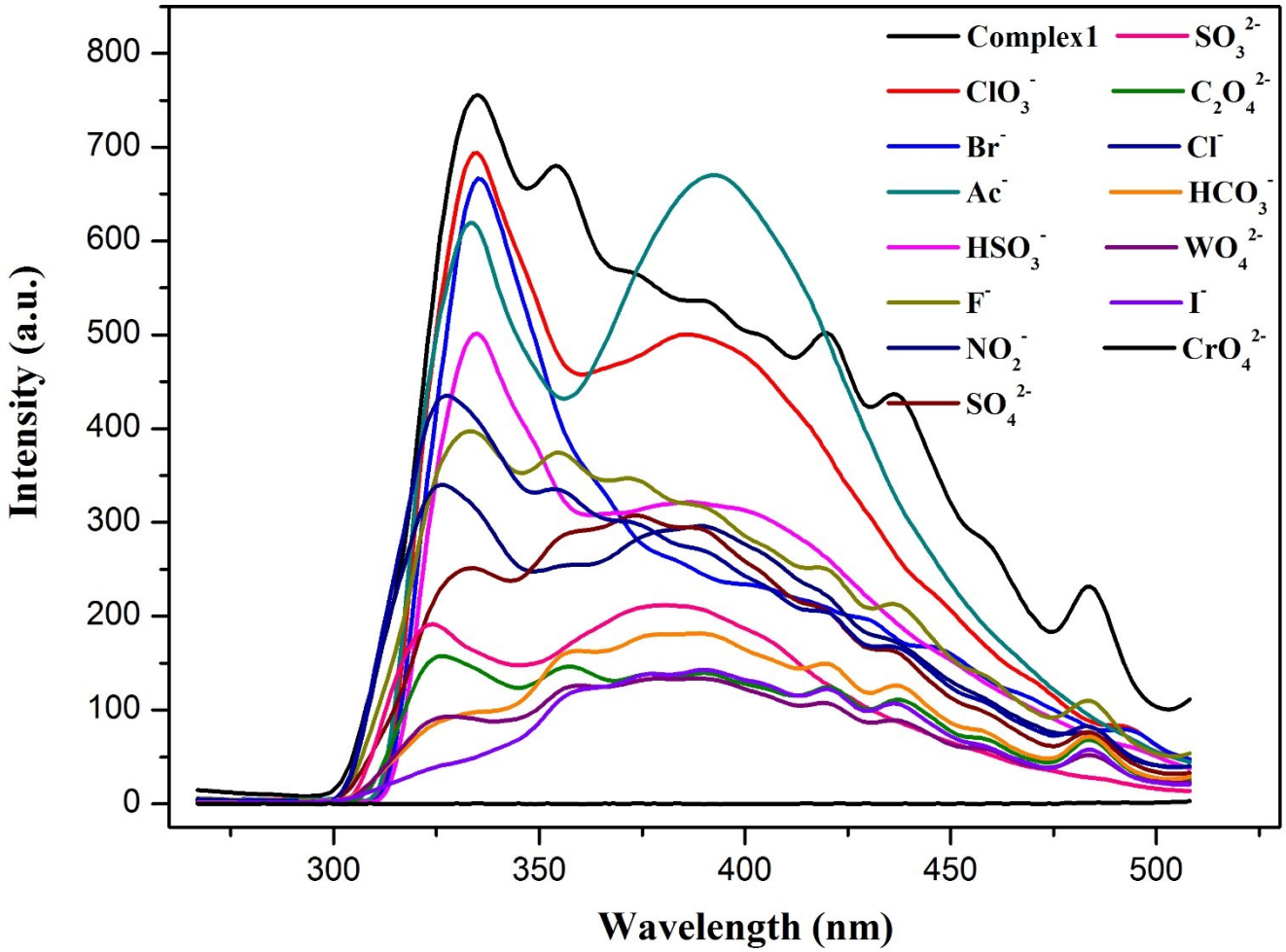

Fig. S5 Emission spectra of **1** with different anions.

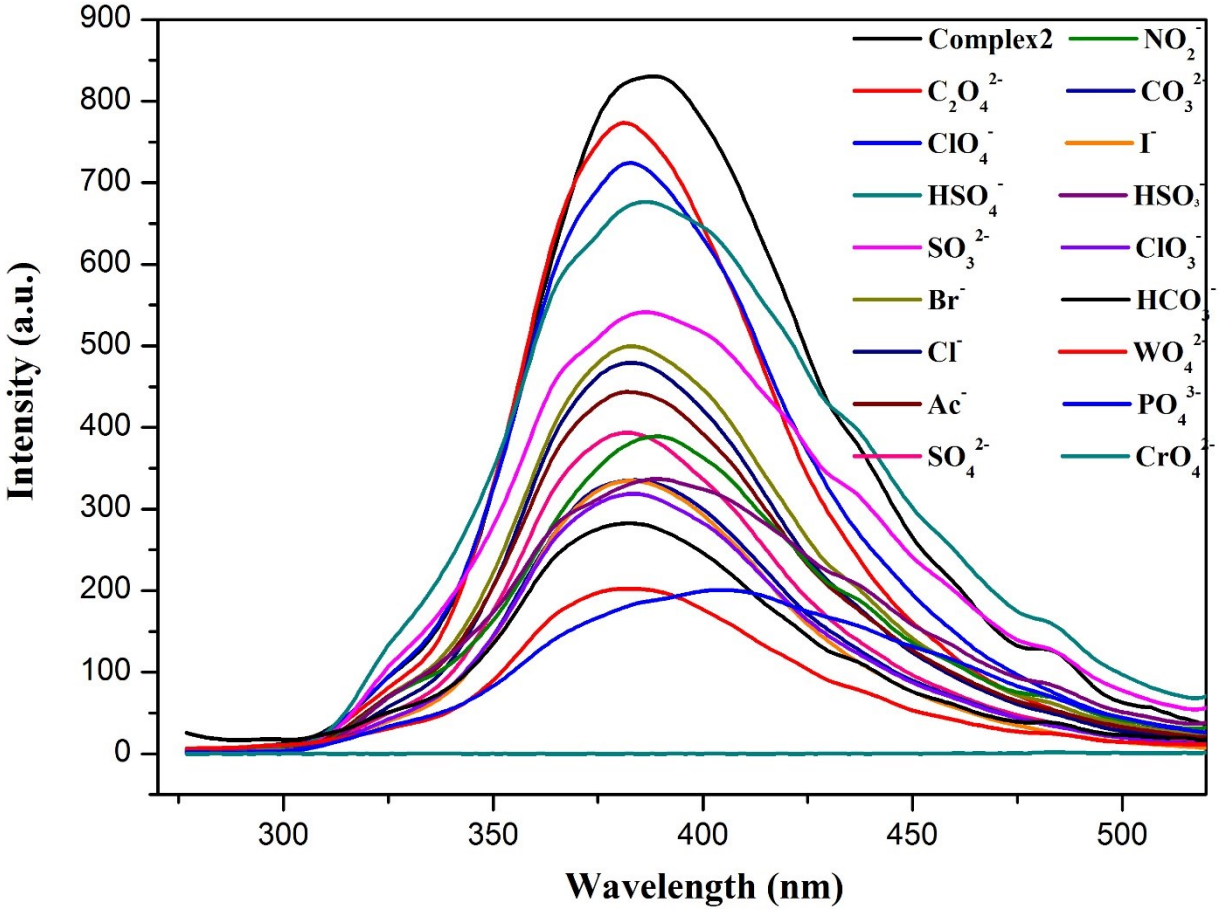

Fig. S6 Emission spectra of **2** with different anions.

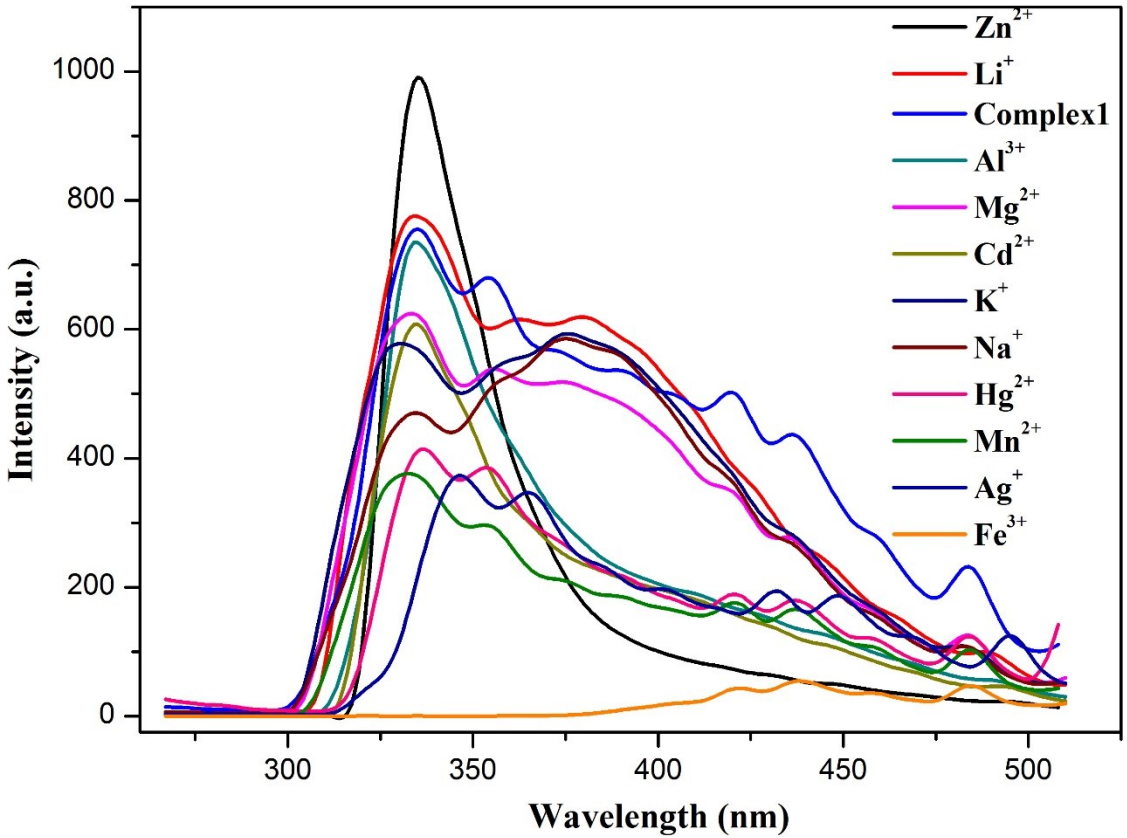

Fig. S7 Emission spectra of **1** with different metal ions.

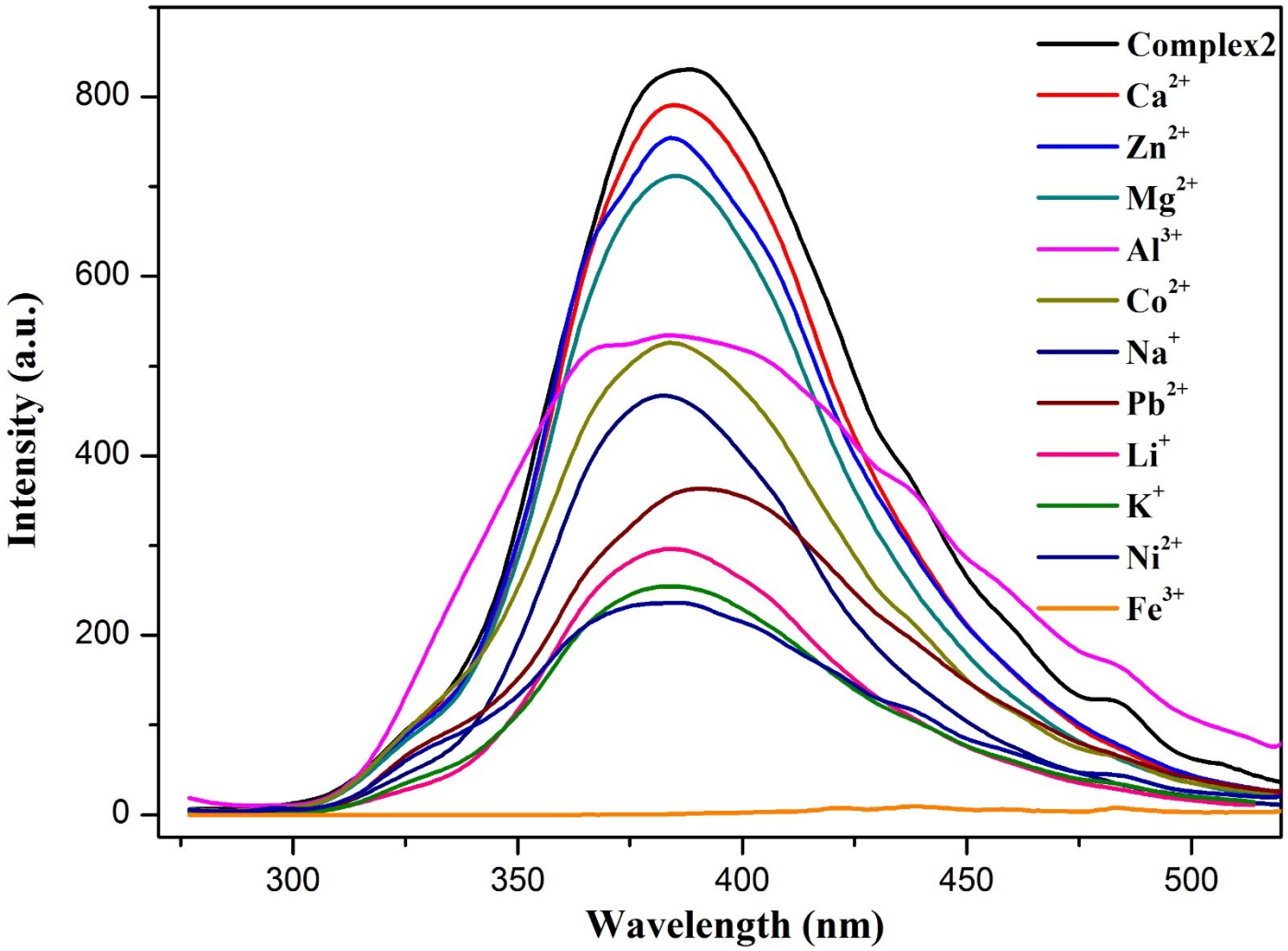

Fig. S8 Emission spectra of **2** with different metal ions.

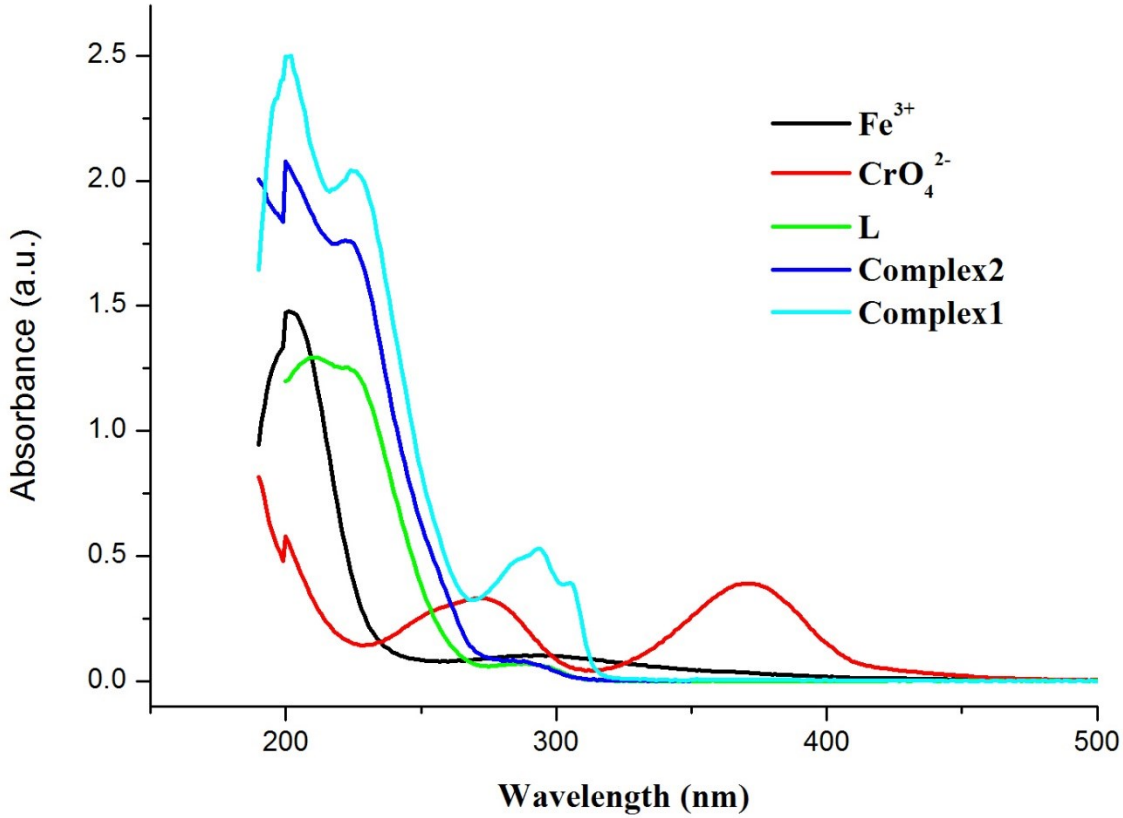

Fig. S9 the UV-vis spectra of complexes and analytes in this work.

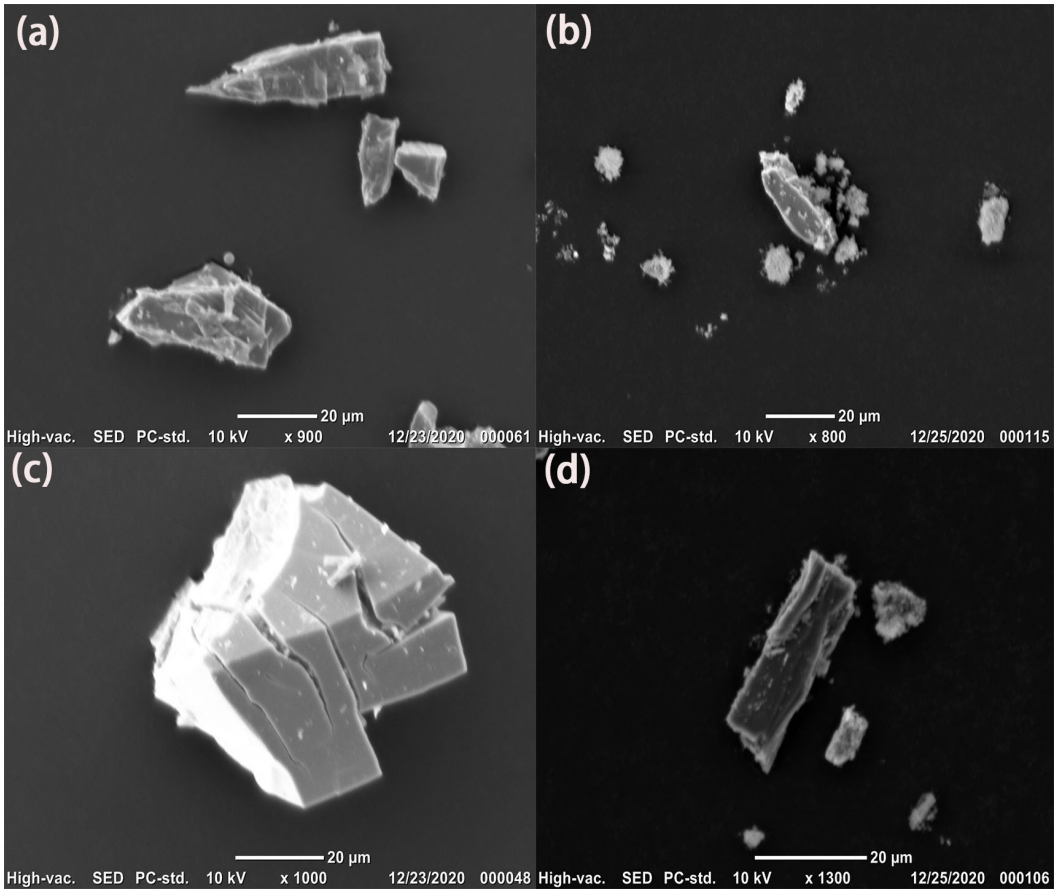

Fig. S10 The SEM images of **1** and **2,** (a) and (c) for the sample after sensing experiment, (b) and (d) for the original sample, respectively.

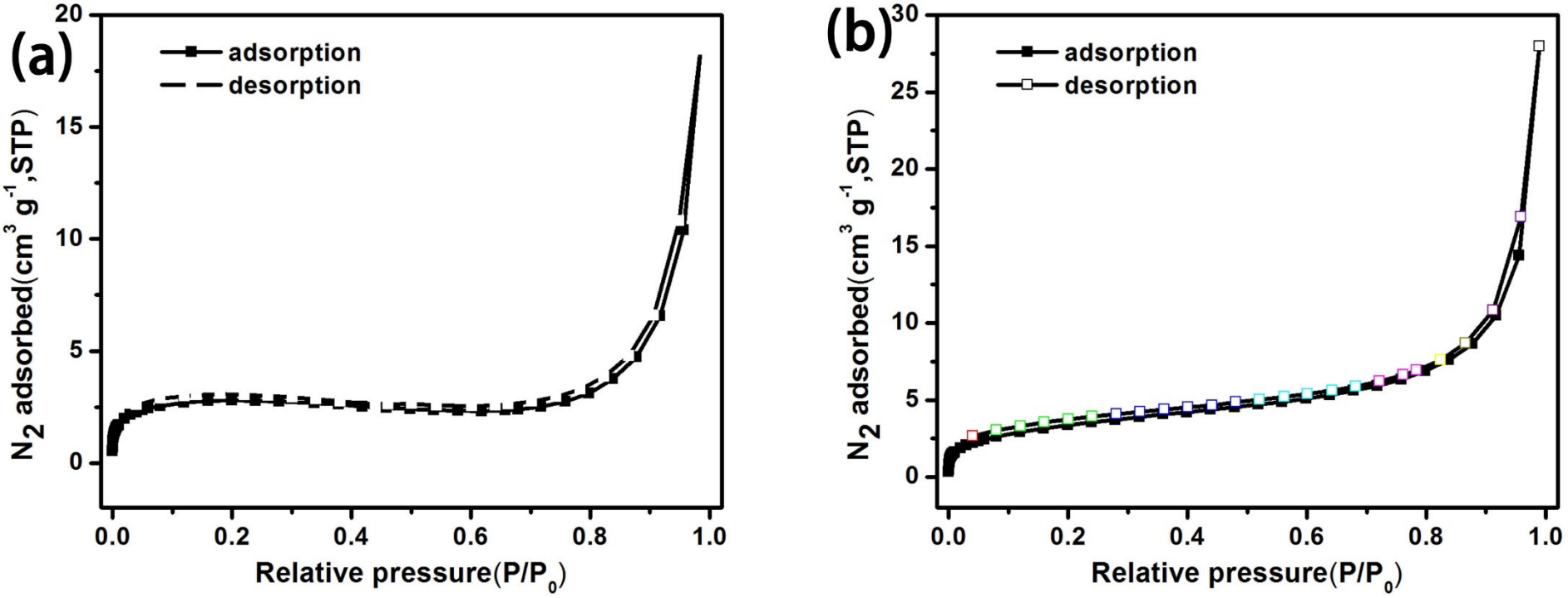

Fig. S11 Nitrogen adsorption-desorption isotherms of **1** and **2**.

Table S1. Crystal data and structure refinement information for **1 and 2**

Parameter	**1**	**2**
Formula	$C_{26}H_{14}Cd_2N_2O_8$	$C_{16}H_{14}Cd_2O_{12}$
Formula weight	707.19	623.07
Crystal system	Triclinic	Monoclinic
Space group	*P*-1	$P2_1/c$
Crystal color	yellow	yellow
a, [Å]	10.1590(8)	7.60650(10)
b, [Å]	11.0042(6)	13.9939(3)
c, [Å]	11.2516(10)	20.8616(4)
α, [°]	74.652(6)	90
β, [°]	66.351(8)	91.090(2)
γ, [°]	79.654(5)	90
V, Å ^{3}	1107.27(16)	2220.20(7)
Z	2	4
ρ_{calcd}, g/cm^3	2.121	1.864
μ, mm^{-1}	15.918	15.872
F(000)	688	1208
θ Range, deg	4.1690- 71.0160	3.804- 71.281
Reflection collected	7126/ 3965	14364/7239

Goodness-of-fit on F^2	1.070	1.068
R_1, $wR_2(I > 2\sigma(I))^*$	0.0456, 0.1148	0.0307, 0.0787
R_1, wR_2 (all data)**	0.0545, 0.1201	0.0370, 0.0811

* $R = \sum(F_o - F_c)/\sum(F_o)$, ** $wR_2 = \{\sum[w(F_o^2 - F_c^2)^2]/\sum(F_o^2)^2\}^{1/2}$.

Table S2. Selected bond distances (Å) and angles (°) of **1**

Cd(1)-O(1)	2.152(4)	Cd(1)-O(3A)	2.178(4)
Cd(1)-O(6B)	2.216(4)	Cd(1)-O(7B)	2.352(4)
Cd(1)-O(7C)	2.308(4)	Cd(2)-O(2D)	2.339(4)
Cd(2)-O(4)	2.297(5)	Cd(2)-O(5E)	2.326(4)
Cd(2)-O(8F)	2.322(4)	Cd(2)-N(1)	2.394(5)
Cd(2)-N(2)	2.347(5)		
O(1)-Cd(1)-O(3A)	90.69(18)	O(1)-Cd(1)-O(6B)	113.44(19)
O(6B)-Cd(1)-O(3A)	108.73(17)	O(7B)-Cd(1)-O(3A)	160.26(17)
O(7B)-Cd(1)-O(7C)	74.07(16)	O(6B)-Cd(1)-O(7C)	76.46(15)
O(2D)-Cd(2)-N(1)	104.70(17)	O(2D)-Cd(2)-N(2)	83.53(17)
O(2D)-Cd(2)-O(4)	161.14(17)	O(5E)-Cd(2)-O(4)	102.96(17)
O(8F)-Cd(2)-O(4)	80.98(17)	N(2)-Cd(2)-O(4)	114.94(17)

Symmetry codes:A: -x, 2-y, 2-z; B: -1+x, y, 1+z; C: 1-x, 2-y, 2-z; D: x, y, -1+z; E: 1-x, 2-y, 1-z; F: -1+x, y, z.

Table S3. Selected bond distances (Å) and angles (°) of **2**

Cd(1)-O(1)	2.251(3)	Cd(1)-O(10)	2.303(4)
Cd(1)-O(3A)	2.319(3)	Cd(1)-O(4A)	2.384(3)
Cd(1)-O(7B)	2.459(3)	Cd(1)-O(8B)	2.396(3)
Cd(1)-O(9)	2.336(5)	Cd(2)-O(2)	2.230(3)
Cd(2)-O(5C)	2.443(3)	Cd(2)-O(6C)	2.323(3)
Cd(2)-O(8B)	2.237(3)	Cd(2)-O(11)	2.335(4)
Cd(2)-O(12)	2.268(4)		

O(1)-Cd(1)-O(3A)	90.22(12)	O(1)-Cd(1)-O(4A)	145.29(12)
O(1)-Cd(1)-O(7B)	132.13(12)	O(1)-Cd(1)-O(8B)	80.18(11)
O(1)-Cd(1)-O(9)	90.5(2)	O(1)-Cd(1)-O(10)	90.81(19)
O(2)-Cd(2)-O(5C)	86.60(11)	O(2)-Cd(2)-O(6C)	135.19(12)
O(2)-Cd(2)-O(8B)	119.63(12)	O(2)-Cd(2)-O(11)	87.45(13)
O(2)-Cd(2)-O(12)	91.89(16)	O(6)-Cd(2)-O(5)	54.76(10)

Symmetry codes:A: -x, 1-y, 1-z; B: -1+x, 0.5-y, -0.5+z; C: x, 0.5-y, -0.5+z.

Table S4 Luminescent sensors for CrO_4^{2-} sensing based on the luminescent MOFs.

MOF	**Solvent**	**Quenching constant, K_{sv}**	**Working range**	**Ref**
$[Zn(L)(H_2O)]\cdot H_2O$	Water	$1.02x10^4$ M^{-1}	0-8 μM	
$[Zn_2(TPOM)(NH_2\text{-}bdc)_2]\cdot 4H_2O$	DMF	$4.45x10^3$ M^{-1}	0-100 μM	
[Zn(IPA)(L)]	Water	$1.00x10^3$ M^{-1}	-	
[Cd(IPA)(L)]	Water	$1.30x10^3$ M^{-1}	-	
$[Eu_2(tpbpc)_4(CO_3)(H_2O)_4]\cdot DMF$	Water	$4.83x10^4$ M^{-1}	0-0.3 mM	
$[Eu_7(mtb)_5(H_2O)_{16}](NO_3)(DMA)_8(H_2O)_{18}$	Water	$3.30x10^4$ M^{-1}	6 nM-2 mM	
[Zn(btz)]	Water	$3.19x10^3$ M^{-1}		
$[Zn_2(ttz)(H_2O)]$	Water	$2.35x10^3$ M^{-1}		
$[Zn_3(bpanth)(oba)_3]\cdot 2DMF$	Water	$1.24x10^5$ M^{-1}	0-3 μM	
$[Y(BTC)(H_2O)_6]_n$:0.1Eu	Water	$1.18x10^3$ M^{-1}	0-300 μM	
$[Zn(NH_2\text{-}bdc)(4,4'\text{-}bpy)]$	Water	$4.56x10^3$ M^{-1}	0-50 μM	
1	Water	$4.51x10^5$ M^{-1}	0-10 μM	This work
2	Water	3.61 $x10^5$ M^{-1}	0-10 uM	This work

References

1. X.-Y. Guo, F. Zhao, J.-J. Liu, Z.-L. Liu and Y.-Q. Wang, An ultrastable zinc(II)–organic framework as a recyclable multi-responsive luminescent sensor for Cr(III), Cr(VI) and 4-nitrophenol in the aqueous phase with high selectivity and sensitivity*, J. Mater. Chem. A*, 2017, 5, 20035–20043.
2. R. Lv, J. Wang, Y. Zhang, H. Li, L. Yang, S. Liao, W. Gu and X. Liu, An amino-decorated dual-functional metal–organic framework for highly selective sensing of Cr(III) and Cr(VI) ions and detection of nitroaromatic explosives, *J. Mater. Chem. A*, 2016, 4, 15494–15500.
3. B. Parmar, Y. Rachuri, K. K. Bisht, R. Laiya and E. Suresh, Mechanochemical and Conventional Synthesis of Zn(II)/Cd(II) Luminescent Coordination Polymers: Dual Sensing Probe for Selective Detection of Chromate Anions and TNP in Aqueous Phase, *Inorg. Chem.*, 2017, 56, 2627–2638.
4. J. Liu, G. Ji, J. Xiao and Z. Liu, Ultrastable 1D Europium Complex for Simultaneous and Quantitative Sensing of Cr(III) and Cr(VI) Ions in Aqueous Solution with High Selectivity and Sensitivity, *Inorg. Chem.*, 2017, 56, 4197- 4205.
5. W. Liu, Y. Wang, Z. Bai, Y. Li, Y. Wang, L. Chen, L. Xu, J. Diwu, Z. Chai and S. Wang, Hydrolytically Stable Luminescent Cationic Metal Organic Framework for Highly Sensitive and Selective Sensing of Chromate Anions in Natural Water Systems, *ACS Appl. Mater. Interfaces*.,2017, 9, 16448–16457.
6. H. R. Fu, Y. Zhao, Z. Zhou, X. G. Yang and L. F. Ma, Neutral ligand TIPA-based two 2D metal–organic frameworks: ultrahigh selectivity of C_2H_2/CH_4 and efficient sensing and sorption of Cr(VI), *Dalton Trans.*, 2018, 47, 3725–3732.
7. G. P. Li, G. Liu, Y. Z. Li, L. Hou, Y. Y. Wang and Z. Zhu, Uncommon Pyrazoyl-Carboxyl Bifunctional Ligand-Based Microporous Lanthanide Systems: Sorption and Luminescent Sensing Properties, *Inorg. Chem.*, 2016, 55, 3952–3959.
8. C. S. Cao, H. C. Hu, H. Xu, W. Z. Qiao and B. Zhao, Two solvent-stable MOFs as a recyclable luminescent probe for detecting dichromate or chromate anions *Cryst Eng.Comm.*, 2016, 18, 4445–4451.
9. L. Wei, H. Xin, X. Cong, C. Chunyang, Y. Lizi, D. Wei, C. Wanmin, Y. Huan and L.Weisheng, A Multi-responsive Regenerable Europium–Organic Framework Luminescent Sensor for Fe^{3+}, Cr^{VI} Anions, and Picric Acid, *Chem. Eur. J.*, 2016, 22, 18769– 18776.
10. Y. Zhao-Quan, L. Guang-Yu, X. Jian, H. Tong-Liang and B. Xian-He, A Water-Stable Luminescent Zn^{II} Metal-Organic Framework as Chemosensor for High-Efficiency Detection of Cr^{VI}-Anions ($Cr_2O_7^{2-}$ and CrO_4^{2-}) in Aqueous Solution, *Chem. Eur. J.*, 2018, 24, 3192–3198.
11. T.W. Duan, B. Yan, H. Weng, Europium Activated Yttrium Hybrid Microporous System for Luminescent Sensing Toxic Anion of Cr (VI) Species, *Microporous Mesoporous Mater.*, 2015, 217, 196-202.

Table S5. A comparison of the Stern-Volmer constant (*K*sv), detection limit used for Fe^{3+} detection for selected MOFs.

No.	Compounds	*K*sv (M^{-1})	detection limit	Ref
1	$[Zr_6O_6(OH)_2(CF_3COO)_2(C_{11}H_5NO_4)_4(H_2O)_4]$	2.25×10^7	1.7×10^{-9}M	1
2	EuL3	4.1×10^3	10^{-4} M	2
3	Eu^{3+}@MIL-124	3.87×10^4	0.28×10^{-6}M	3
4	Tb^{3+}@Cd-MOF	1.108×10^5	0.010 mM	4
5	$[Zr_6O_4(OH)_4(2,7\text{-CDC})_6]$	5.5×10^3	9.10×10^{-7}M	5
6	**1**	2.99×10^5	2.47×10^{-8}M	This work
7	**2**	1.23×10^6	1.35×10^{-9}M	This work

References:

1. C. Gogoi, S. Biswas, *Dalton Trans*. 2018, 47, 14696
2. M. Zheng, H. Tan, Z. Xie, L. Zhang, X. Jing and Z. Sun, *ACS Appl. Mater. Interfaces*, 2013, 5, 1078−1083.
3. X.-Y. Xu and B. Yan, *ACS Appl. Mater. Interfaces*, 2014, 7, 721-729.
4. H. Weng and B. Yan, *Sens. Actuator B-Chem.*, 2016, 228, 702–708.
5. A. Das and S. Biswas, *Sens. Actuator B-Chem*, 2017, 250, 121-131.